Chinese Journal of
POLYMER SCIENCE

RESEARCH ARTICLE

https://doi.org/10.1007/s10118-022-2712-6
Chinese J. Polym. Sci. **2022**, *40*, 642–650

Shape Accuracy and Residual Stress Distribution of Nano-molded Semicrystalline Polymer: A Simulation Study

Dan Xu[a], Yu-Yuan Lu[a,b*], and Chuan-Fu Luo[a,b*]

[a] *State Key Laboratory of Polymer Physics and Chemistry, Changchun Institute of Applied Chemistry, Chinese Academy of Sciences, Changchun 130022, China*
[b] *University of Science and Technology of China, School of Applied Chemistry and Engineering, Hefei 230026, China*

Electronic Supplementary Information

Abstract The shape accuracy and residual stress distribution of a nano-molded semicrystalline polymer are studied by molecular dynamics simulations. Semicrystalline polyethylene flakes are obtained by continuous cooling inside templates with four shapes. We find that the curvature of contour curve near template corners decreases with corner angle. A simple 2D shape model of minimum surface energy is proposed to understand the shapes for repulsive and attractive templates. The confinement of template induces highly ordered chain packing in surface region. According to the spacial distribution of local stress, we find the contracting stress caused by volume shrinkage during cooling concentrates on the chains perpendicular to the direction of relative stress principal. The distribution of von Mises stress indicates the outer layer of semicrystalline polymer flake has lower distortion. Our results provide a theoretical insight for better nano-molding techniques.

Keywords Polymer semi-crystallization; Molecular dynamics simulation; Template

Citation: Xu, D.; Lu, Y. Y.; Luo, C. F. Shape accuracy and residual stress distribution of nano-molded semicrystalline polymer: a simulation study. *Chinese J. Polym. Sci.* **2022**, *40*, 642–650.

INTRODUCTION

Crystallization of polymer materials under nanoscopic confinement is highly concerned in nanotechnology.[1–7] Due to diverse requirements of industrial applications and research focuses in experiments, the nanoscopic products or experimental samples have different shapes and properties. The typical materials to confine polymers at the nanoscale are provided by aluminum anodic oxide (AAO),[8–11] or by the microdomain structures formed through microphase separation of block copolymers, *etc*.[7,12–14] Studies on the flow behaviors of polymers in nanochannels were reported,[15] by using infiltrated nanochannels because polymer melts could wet and flow in nanochannels rapidly at a temperature much higher than the melting point. A silicon mold with the width of the trenches ranges from 40 nm to 250 nm is expected to be small enough to influence the polymer crystallization but large enough for keeping crystalline superstructure of polymers.[4] Usually, the existence of templates changes crystallization behavior including nucleation mechanism, crystal orientation, crystallization kinetics, and polymorphic transition, *etc*.[8] Woo *et al*.[16] studied the crystallization of linear polyethylene (PE) infiltrated in AAO templates. They found that the crystallization temperature (T_c) decreases with pore size, and the degree of crystallinity is generally lower for infiltrated polymers within AAO nanopores than that for neat bulk polymers.[17,18] For the chain arrangement in AAO nanopores, a parallel nucleus is formed at the surface of nanopore wall when the size of pores becomes as small as 32–80 nm.[19] It is demonstrated that crystallinity influences the formationoffrozenlayer,theinternalstresses,andthein-moldshrinkage.[20,21] The investigation of how thermal stress induced by the coefficient of thermal expansion affects the glass transition behavior of polystyrene (PS) nanorods located inside cylindrical AAOnanoporesrevealsstressisacomplexandimportantroleinconfinement condition.[22]

Computer simulation can be used as an adminicular method to study polymer crystallization under confinement, since it can provide a unique microscopic insight into the structures, dynamics and forces arising from the crystallization process.[23–29] In this study, we carry out molecular dynamics (MD) simulations to study the crystallization of PE aggregates inside a sealed three dimensional (3D) template. The accuracy of template becomes worse as the size decreases due to the limited processing precision at the nanoscale.[30] It is known that the cooling process to form semi-crystals causes volume collapse will affect the dimension accuracy of a nano-molded polymer product.[31] As shape accuracy and mechanical properties are of the most importance for a nanoscopic product, our study will focus on the shape accuracy and the residual stress distribution of nano-molded semicrystalline polymer

* Corresponding authors, E-mail: yylu@ciac.ac.cn (Y.Y.L.)
E-mail: luocf@ciac.ac.cn (C.F.L.)

Special Issue: Ordered Structure of Polymers
Received December 31, 2021; Accepted February 7, 2022; Published online April 22, 2022

© Chinese Chemical Society
Institute of Chemistry, Chinese Academy of Sciences

flakes formed inside templates. Here, we design four shaped templates with different corners to study the shape accuracy affected by corners of templates. We will study the crystalline structure, chain orientation, and local stress distribution of the semicrystalline polymer flakes.

MODEL AND METHOD

We use MD simulation with united atom (UA) model to study the shape accuracy and residual stress distribution of a nano-molded semicrystalline polyethylene (PE) flake. For PE chains, each methylene or methyl unit (CH_2 or CH_3) is treated as a bead and the beads along a chain are connected by springs. The interactions between beads are modeled by bonded (bond, angle, and dihedral) and non-bonded (van der Waals) potentials. The parameters proposed by Rigby *et al.*[32,33] are used in this study. The classical Lennard-Jones (LJ) potential $U(r) = 4\varepsilon[(\sigma/r)^{12} - (\sigma/r)^6]$ with σ=0.38 nm and ε=0.5 kJ/mol is used to model the van der Waals interaction between two polymer beads separated by a distance of r. The cut-off distance of the LJ potential is 0.95 nm, which equals to 2.5σ. In the UA model, the flexibility of a PE chain is dominated by the dihedral potential which reflects the degree of rotational freedom. The bond and angle potentials determine the local structure and size of a short segment. The template is modeled by particles connected through hard springs, and the interaction between template particles and polymer beads are modeled by a LJ potential. The template particles are aligned according to the cubic lattice with distance of 0.5 nm (the lattice distance in cylindrical template is 0.4 nm to ensure the resolution of a circle shape). The interaction between polymer beads and template particles is also modeled by the LJ potential with σ=σ'=0.38 nm. The template behaves as a repulsive wall if ε'=0.07 kJ/mol, while as an attractive wall if ε=ε'=0.5 kJ/mol. An illustration of a PE chain represented by UA model and the interaction between polymer beads and template particles are shown in the insets of Fig. 1(d).

We use the GROMACS (version 2019.3)[34] software to do our simulations, which is a fast MD code with acceleration of GPU and is widely used in simulations of macromolecules.[35,36] A conventional leapfrog integration method with a time step of 5 fs is applied in this study and the temperature (T) is controlled by the *v-rescale* method. The *v-rescale* algorithm in GROMACS includes a stochastic term and can generate a conformation with proper ergodicity.

In this study, the polymer aggregates consist of 300 PE chains with chain length N=200 (number of C atoms). We carry out simulations by the following process, as illustrated in Figs. 1(a)–1(c): Firstly, the polymer aggregates are melted and relaxed under T=600 K for 50 ns and then put into the template. Secondly, the top flat board is pushed down to make the inside volume reach the target value, 1860 nm^3, which corresponds to the density of PE chains at T=600 K and 1 bar by using the same UA model. Considering that there is a surface repulsion layer with a size about σ, the equivalent density of the inside polymer aggregates is related to a PE melt at T=600 K and high pressure (estimated about 100 bar). Finally, the polymer aggregates are cooled from T=600 K (melt) to 150 K (semicrystal) in 100 ns with fixed template volume. We use two kinds of templates (repulsive and attractive) to do the simulations, as mentioned above and shown in Fig. 1(d). Two snapshots of the semicrystalline polymer inside a repulsive template after cooling are shown in the right panel of Fig. 1(c). To do further analysis, the semicrystalline flake is taken out from the template and is further relaxed at T= 300 K for a short time of 1 ns. For each condition, five inde-

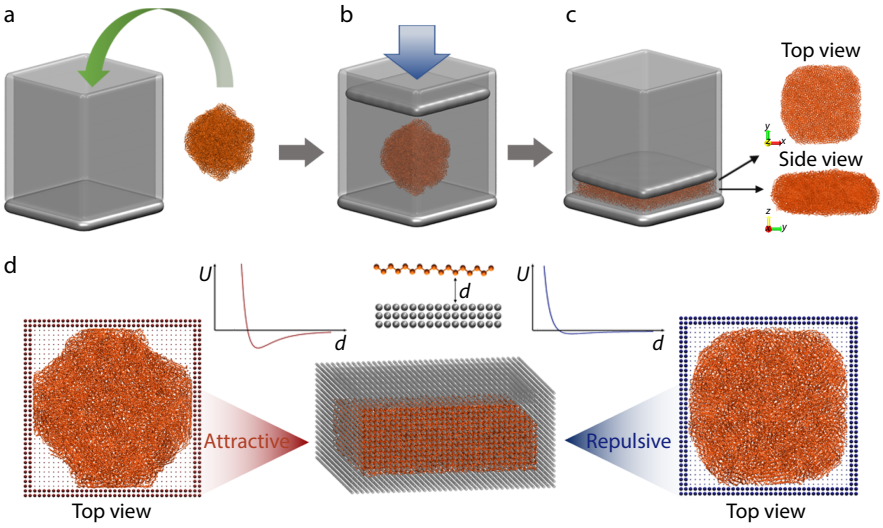


Fig. 1 Flow chart of simulation process and illustration of studied systems. (a) Putting polymer aggregates (in melt state) into a template which is drawn by transparency method for visual clarity. (b) Pushing the top board down to make the volume inside the template reaches the target one. (c) Cooling polymer aggregates inside the template. The right two snapshots are the top- and slice-view of the semicrystalline polymer after cooling, of which the structural properties and residual stress are analyzed further. (d) Initial melt configuration of polymer aggregates inside the template in 3D view (middle), snapshots of semicrystalline polymer inside an attractive template (left) and repulsive one (right) viewed from the top. Here, the attractive and repulsive templates are drawn in orange and blue colors, respectively. Insets illustrate the UA model for a PE chain and the LJ potential (U) between polymer beads and template particles versus distance (d).

https://doi.org/10.1007/s10118-022-2712-6

pendent runs (ensemble samples) are performed to obtain more reliable results.

RESULTS AND DISCUSSION

In order to study the semicrystalline structure of PE chains under nano-confinement, we studied four shapes of model templates, of which the top views along *z*-direction are shown in Fig. 2. Both repulsive and attractive walls mentioned above are studied, and the snapshots of semicrystalline polymer aggregates obtained from continuous cooling are also shown in Fig. 2. The inner length of template side boards in Figs. 2(a), 2(c) and 2(d) is 20 nm and the diameter of cylindrical template in Fig. 2(b) is 20 nm, respectively. Cooling and crystallization processes cause volume shrinkage of the polymer aggregates and create vacancies inside the template. Shapes of semicrystalline PE flakes are different according to attractive or repulsive templates. For convenience of discussion, we first discuss the results of repulsive templates, which could be the common situation for a real nano-molding.

When the template repels polymers, the semicrystalline polymer aggregates collapse inward away from the template surface, as shown in Figs. 2(a)–2(d). The shape of semicrystalline polymer flakes inside repulsive templates is rather symmetrical and the interface is gentler than those in attractive condition as shown in Figs. 2(e)–2(h). If the template is cylindrical, the semicrystalline polymer flakes show a circular shape in *xy*-plane. When the templates have corners as shown in Figs. 2(a), 2(c) and 2(d), vacancies exist near template corners and the shape curve of semicrystalline polymer flakes near the corners is convex. From Figs. 2(c) and 2(d), we can see that the vacancies at acute corners of the templates are apparently larger than those at obtuse corners. We note that all five independent runs have the same conclusion about the shape of semicrystalline polymer flakes inside the repulsive templates.

In order to accurately describe the shape characteristics of the semicrystalline polymer, we apply the snake model[37] to find the two dimensional contour of semicrystalline polymer aggregates mapped to the *xy*-plane as shown in Fig. 3. A snake denoted by the blue contour in Fig. 3(b) is an energy-minimizing spline subjected to image forces which pull the snake toward or push the snake away from the image features such as edges and lines denoted by the black region in Fig. 3(b). Here, the results of five independent samples are applied. We use the *active-contour* algorithm in the "scikit-image" package, and the parameters of snake model are chosen as ω_{line}=0, ω_{edge}=1, α=0.015, β=10 and γ=0.001. We truncate the contour curve near the template corners and fit the curve to parabola functions as shown in Figs. 3(c) and 3(d). The curvature of this truncated contour is calculated as $\kappa=2a$, where a is the parameter in a parabolic equation: $y = ax^2 + bx + c$ or $x = ay^2 + by + c$. We note here that other fitting curves such as a circular arc or a hyper ellipse does not get a better fitting than the parabolic curve.

We plot the contour curvatures (κ) of the semicrystalline polymer aggregates closed to the template corners versus the respective corner angles (θ) at different temperatures during cooling (400 K, 275 K, 150 K) in Fig. 4. There are five values of corner angles in our simulations: θ=60° corresponds to the left and right corners of template-4, θ=75° corresponds to the left and right corners of template-3, θ=90° corresponds to the corners of template-1, θ=105° corresponds to the top and bottom corners of template-3, and θ=120° corresponds to the top and bottom corners of template-4, respectively. We can see that κ decreases during cooling at all the five corner angles, indicating that the free surfaces of semicrystalline polymer aggregate at corners change towards flat due to volume shrinkage. Thus, the final shape of semicrystalline polymer flakes is blunter than the template. The contour curvature of semicrystalline polymer aggregates close to obtuse angles is found smaller than that close to acute angles, reflected by that κ decreases as θ. For example, θ=60° and θ=120° in Fig. 4 correspond to the left acute corner and the top obtuse one of template-4, where κ=0.35 and κ=0.13 at

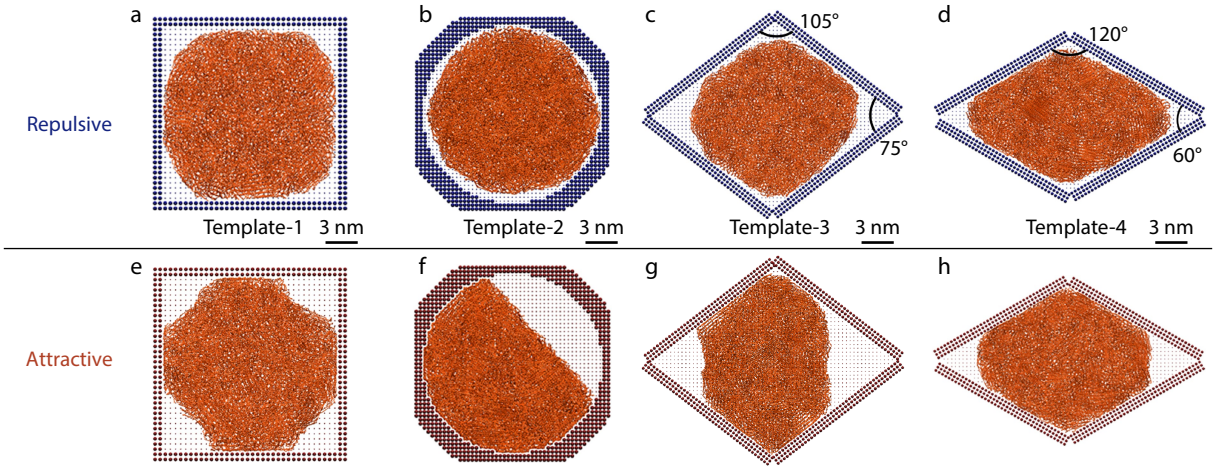


Fig. 2 (a–d) Polymer aggregates reaching semicrystalline state at T=150 K confined in repulsive template. We name the four templates with different shapes as "template-1", "template-2", "template-3" and "template-4". (e–h) Semicrystalline polymer aggregates confined in attractive templates at T=150 K. Snapshots are the top view along *z*-axis. The top flat board of the template is hidden and the bottom board is shown in small dots for visual clarity.

https://doi.org/10.1007/s10118-022-2712-6

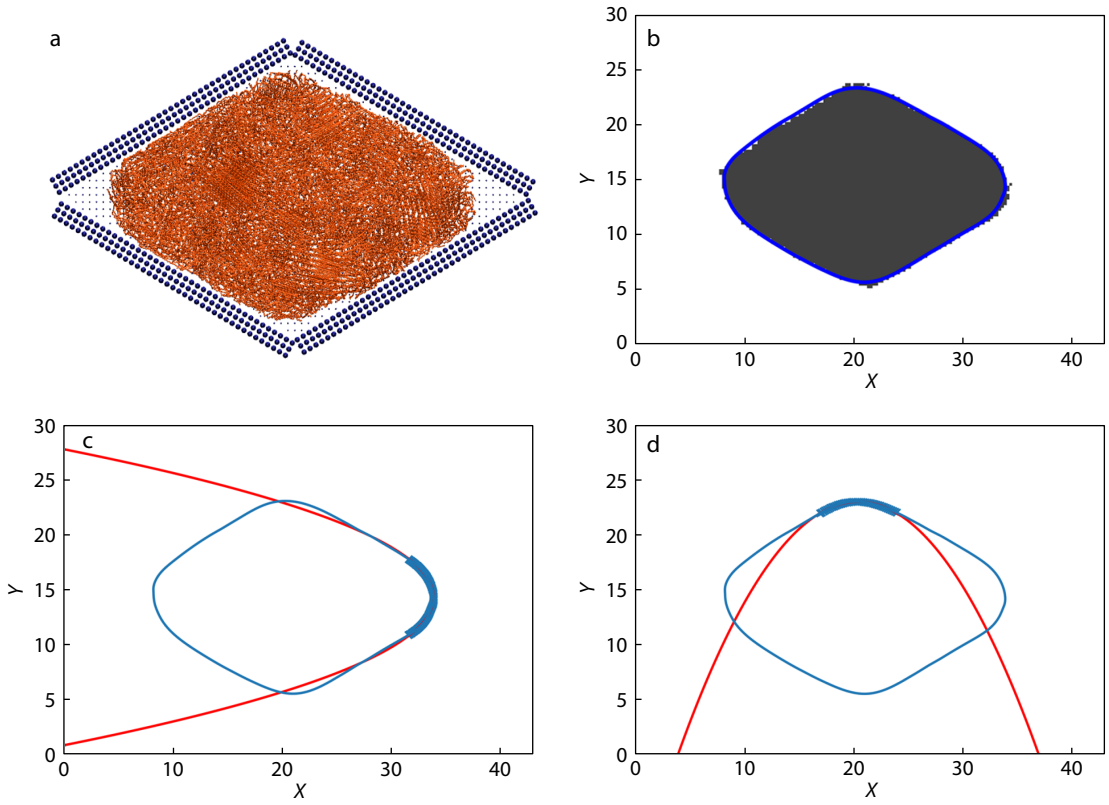


Fig. 3 (a) One snapshot of semicrystalline polymer confined in repulsive template-4 at T=150 K. (b) Projected polymer positions in xy-plane and its contour curve. Here, the projected positions are obtained from five independent runs and the blue contour curve is calculated by the "active-contour" algorithm. (c, d) Parabolic fitting for corners. The bold part of the contour is used to fit the parabolic equation, and the red curve denotes the parabola after fitting.

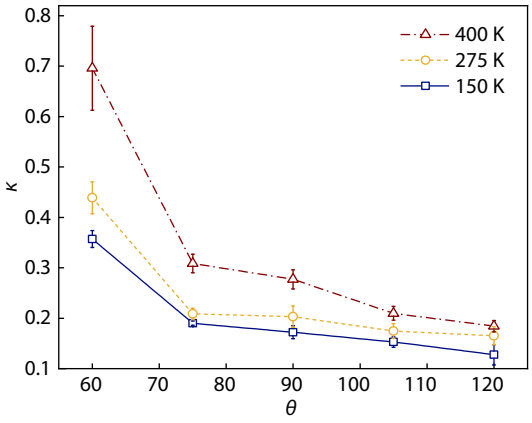


Fig. 4 Contour curvatures (κ) of semicrystalline polymers versus relative angles of template corners (θ) at different temperatures during cooling (400 K, 275 K, 150 K), for repulsive templates

T=150 K, respectively. We also notice the change of κ during the cooling process from 400 K to 150 K at θ=60° is larger than that at θ=120°, which means the polymers close to smaller angled corners collapse more severely during the cooling process. Because obtuse angles of the template are easier to be infiltrated than acute angles.

In literature, researchers used diverse order parameters which reflect the ordering of particles to characterize crystal structures, such as the order parameter $Q_6 = Q_{l=6}(i)$ for the i^{th} particle, defined as:[38,39]

$$Q_l(i) = \left(\frac{4\pi}{2l+1} \sum_{m=-l}^{l} |\bar{q}_{lm}(i)|^2 \right)^{1/2} \quad (1)$$

$$\bar{q}_{lm}(i) = \frac{1}{\tilde{N}_b(i)} \sum_{k=0}^{\tilde{N}_b(i)} q_{lm}(k) \quad (2)$$

where q_{lm} are the spherical harmonics and $\tilde{N}_b(i)$ is the number of neighboring beads of the i^{th} bead including itself. Q_6 is a conventional measurement of the local structure around a particle, which is constructed based on spherical harmonics and reflect the spatial symmetry of particle positions. We use the order parameter Q_6 to characterize the arrangement of polymer beads and the local crystallinity of semicrystalline polymer flakes. The cut-off distance of $\tilde{N}_b(i)$ we choose here is 0.74 nm. We also calculate the entanglement length N_e to describe the inter-chain topology of semicrystalline polymer chains.[40] The calculation of N_e is based on Primitive Path Analysis (PPA) of chain entanglements.[41] The basic idea of PPA is to let polymer chains shrink with fixed ends without chain crossing, which results in primitive paths consisting of kinks and straight segments. The straight segment could be identified by the bending angles greater than 175° between two adjacent kinks in a primitive path, and the number of beads in the straight segment could be used to calculate the local entanglement length. Here, all beads in the same straight segment are assig-

ned by the same N_e value, denoted as $N_e(i)$ for the i^{th} bead.

To discuss the arrangement characteristics of semicrystalline polymer aggregates inside templates, we show the snapshot of Q_6 and N_e in Fig. 5, where the top and middle slices of both Q_6 and N_e in different templates are displayed. An illustration of top and middle slices is displayed in Fig. 6. The top and bottom boards of the template in *xy*-plane cause the structure difference between surface and inside regions of polymers, as shown in Fig. 5(a). We can see from Figs. 5(a), 5(c), 5(e) and 5(g) that in the top slice, Q_6 is higher in the regions where polymer chains are regularly arranged than that in the regions where polymer chains arrange randomly. Comparing the distribution of Q_6 in the top slice with the middle one, we can see chains in the surface layer (top slice) arrange more regularly than that in the middle one. This result indicates an enhancement of crystallization due to the confinement effect of templates. Comparing the distributions of Q_6 and N_e, we can see that most crystalline regions with higher Q_6 have higher N_e too, where chains are regularly folded. Q_6 and N_e match well in some crystalline regions, for example the region noted by red circles in Figs. 5(c) and 5(d). For total space of both top and middle slices, Q_6 and N_e exhibit a weak but notable correlation. This phenomenon shows regularly arranged chains are less tangled in the surface region and the template board enhances the regularity of chain arrangement, which is consistent with our previous simulations of coarse-gained polymers confined within two plane walls.[42]

The chain arrangement and orientation in the top and middle slices are different, indicated by the Q_6 in Fig. 5. It is clear that chains in the top slices are more aligned in *xy*-plane, from the chain conformations of two thin slices shown in Figs. 6(a) and 6(b). Due to the confinement of template boards, polymer chains form oriented folded structure during crystallization. To analyze the chain orientation, we calculate the Herman's bond orientational order parameter along *z*-direction by:

$$P_z = \frac{1}{2}\left(3\left\langle\cos^2\phi\right\rangle - 1\right) \tag{3}$$

where ϕ is the angle enclosed by a bond direction and the *z*-axis. We define $\overrightarrow{C_{ij}}$ the vector from bead *i* to bead *j* in a polymer chain. Because beads in the UA model of a PE chain take a zigzag conformation, we calculate the bond orientation for every two carbon-carbon bonds, as $\overrightarrow{C_{13}}$, $\overrightarrow{C_{24}}$, $\overrightarrow{C_{35}}$, $\overrightarrow{C_{46}}$··· The order parameter P_z can take values between −0.5 and 1. If all the bonds are aligned along the *z*-direction, then P_z=1; If all bonds are in random directions, then P_z=0; If all bonds are perpendicular to the *z*-direction, then P_z=−0.5. We plot P_z versus normalized *z* direction of the semicrystalline polymer flakes in four repulsive templates in Fig. 6(c). We can see the four curves show the same tendency: P_z comes up to the highest value in the middle *z* region and reaches the minimum value when *z* approaches 0 or 1. The minimum value of P_z is close but slightly

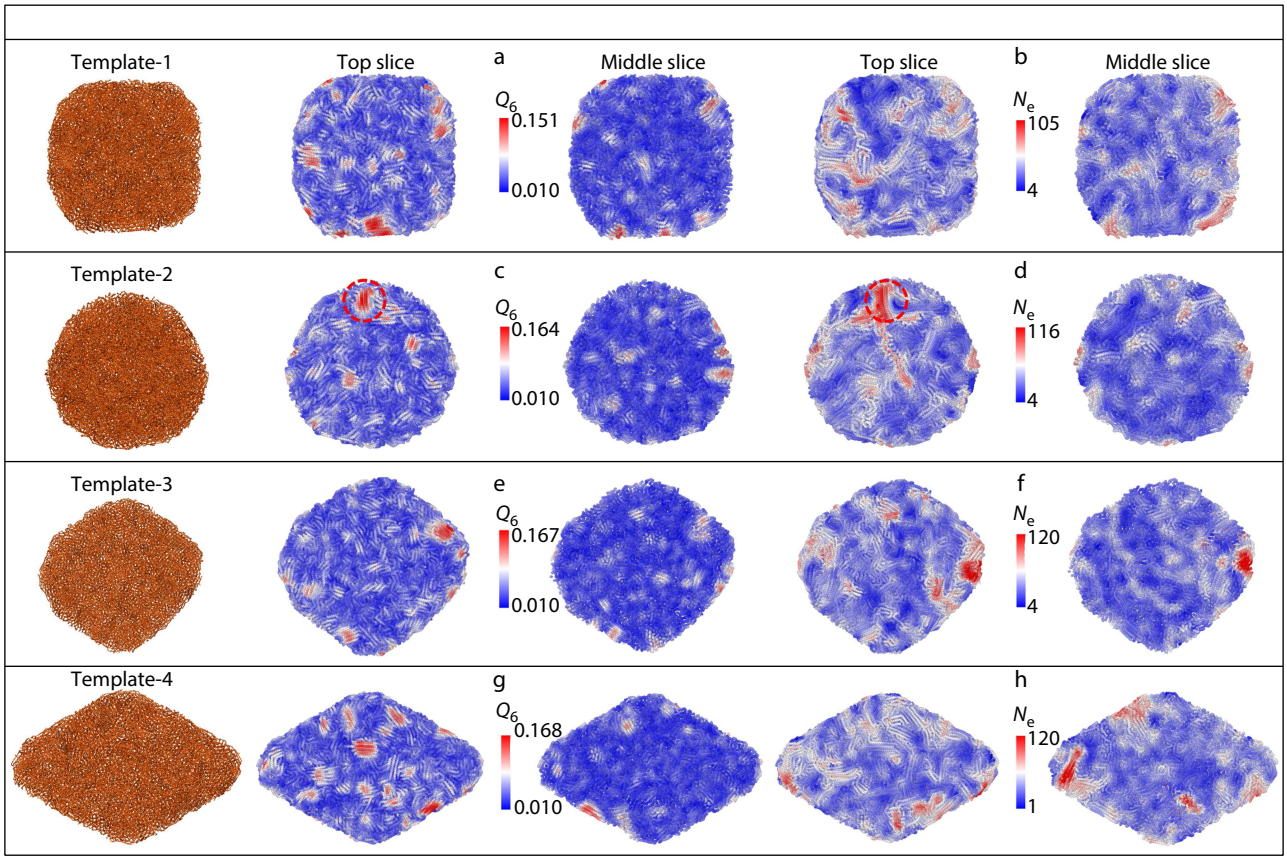


Fig. 5 Top and middle slices of both Q_6 and N_e of semicrystalline polymer aggregates in four different repulsive templates. The structures of semicrystalline polymer chains are shown in the left column by the orange color. We calculate Q_6 and N_e only for polymer beads by taking them out from the templates. The red dashed circles denote the areas with high regularity of chain packing, in which Q_6 and N_e are relatively higher.

https://doi.org/10.1007/s10118-022-2712-6

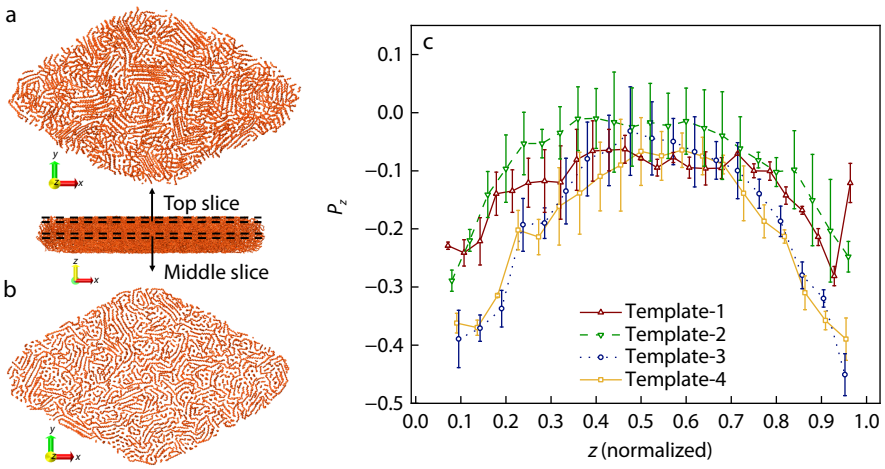


Fig. 6 (a, b) Top and middle slices of a semicrystalline polymer aggregate in *xy*-plane, for repulsive templates; (c) Herman's bond-orientation order parameter along *z*-direction (P_z) versus normalized thickness of polymer aggregates in *z*-direction. The result is averaged from five independent runs.

higher than −0.5, indicating chains near the top and bottom surfaces arrange perpendicularly to *z*-axis (*i.e.*, in *xy*-plane). The highest value of P_z is slightly lower than 0. This does not mean the chains are in amorphous structure but means that the orientations of small crystallites are in nearly random directions. We note that *P* is still negative even in the middle region, since the thickness (in *z*-direction) of the semicrystalline flakes is small compared to the radius of gyration for polymer chains and the chain orientations are affected by the confinement effect for the whole aggregates.

Residual stress is an important property which affects the application of a nano-molded product. However, the residual stress is very difficult to detect in experiments, especially at the nanometer scale. Here, we study the local stress distribution of the semicrystalline polymer aggregates and a result for the repulsive template-4 is shown in Fig. 7. One would expect that the local stress distribution is not only affected by the crystalline-amorphous regions but also the template, due to the confinement of templates. The calculations of local stress tensor are performed with the GROMACS-LS 4.5.5 package.[43,44] We calculate the stress principals in *x*-direction (σ_{xx}), *y*-direction (σ_{yy}), *z*-direction (σ_{zz}) and the von Mises stress (σ_v). The stress principals are the diagonal elements of the Cauchy's stress tensor and can reflect the compress-stretch condition of a given polymer region. The von Mises stress (σ_v) reflects the shear deformation of the relative region and is usually used to predict the yielding of plastic materials under multiaxial 3D loadings. It is defined as:

$$\sigma_v = \sqrt{\frac{3}{2} s_{ij} s_{ij}} \tag{4}$$

where s_{ij} is components of stress deviator tensor σ_{dev}:

$$s = \sigma_{\text{dev}} = \sigma - \frac{\text{tr}(\sigma)}{3} I \tag{5}$$

We show the local stress distribution according to beads of the top and middle slices respectively in Fig. 7, similar to the above treatment to show the structural difference between surface and inside layers. In the top slice perspective, σ_{xx} is smaller if chains arrange along *x*-axis (blue dashed circle in Fig. 7a), and σ_{xx} is larger if chains arrange along *y*-axis (red dashed circle in Fig. 7a). Identically, σ_{yy} is smaller if chains arrange along *y*-axis (blue dashed circle in Fig. 7c), and σ_{yy} is larger if chains arrange along *x*-axis (red dashed circle in Fig. 7c). This phenomenon shows that the contraction force along the *x*-direction acts on the chains which arrange perpendicular to the *x*-direction, and this rule also applies to the contraction force along the *y*-direction. We can see that von Mises stress σ_v in the top slice in Fig. 7(g) and the side surface at the contour in Fig. 7(h) is lower, and σ_v in the middle of semicrystalline polymer aggregates is higher. This means the outer layer of semicrystalline polymer flakes has lower distortion, probably due to those chains in a surface region can relax their conformations easier than those in the inside region. Our results of local stress distribution shown anisotropic properties related to the chain conformations but no obvious effect of templates. Further investigations according to the relation between local stress distribution and chain structure are needed in our future work.

When the template attracts polymers, the shape of semicrystalline polymer flakes is less regular than that of repulsive templates, as shown in Figs. 2(e)–2(h). As the existence of attraction between template particles and polymer beads, the polymer aggregates would prefer to contact larger template surface during the shrinkage caused by cooling. For an attractive cylinder template, the contour shape in *xy*-plane is a cut circle with a straight line, as shown in Fig. 2(f). For attractive cornered templates, the vacancies near corners are respectively larger than that in repulsive templates and the contour curve near corners becomes concave.

To give a simple understanding of the shape for semicrystalline polymer aggregates inside templates, a simple 2D shape model is proposed as illustrated in Fig. 8(a). The contour of polymer aggregates is divided into lines (L_i) contacting with the inner surface of a template and curves (C_i) near the template corners. The final shape is determined by the polymer-template interaction and surface tension at a given volume (area in the 2D model) under the confinement of templates. This is an optimization problem to find a contour curve $\Omega = y(x)$ with the minimum of surface energy $f[\Omega]$:

$$\min_{\text{sub},A_\Omega=A_0,\Omega\subset\Gamma} f[\Omega] = \sum_{i=1}^{4} (\eta L_i + C_i) \quad (6)$$

where Ω is the contour consists of L_i and C_i confined in the template region Γ. The area inside the contour is A_Ω which should be constrained as a constant A_0 according to the shrinking rate. The parameter η reflects the relative interaction between polymers and template surface. The template is repulsive if η>1, and attractive if η<1. The minimization can be done numerically and the final contour curves are displayed in Fig. 8(b) for

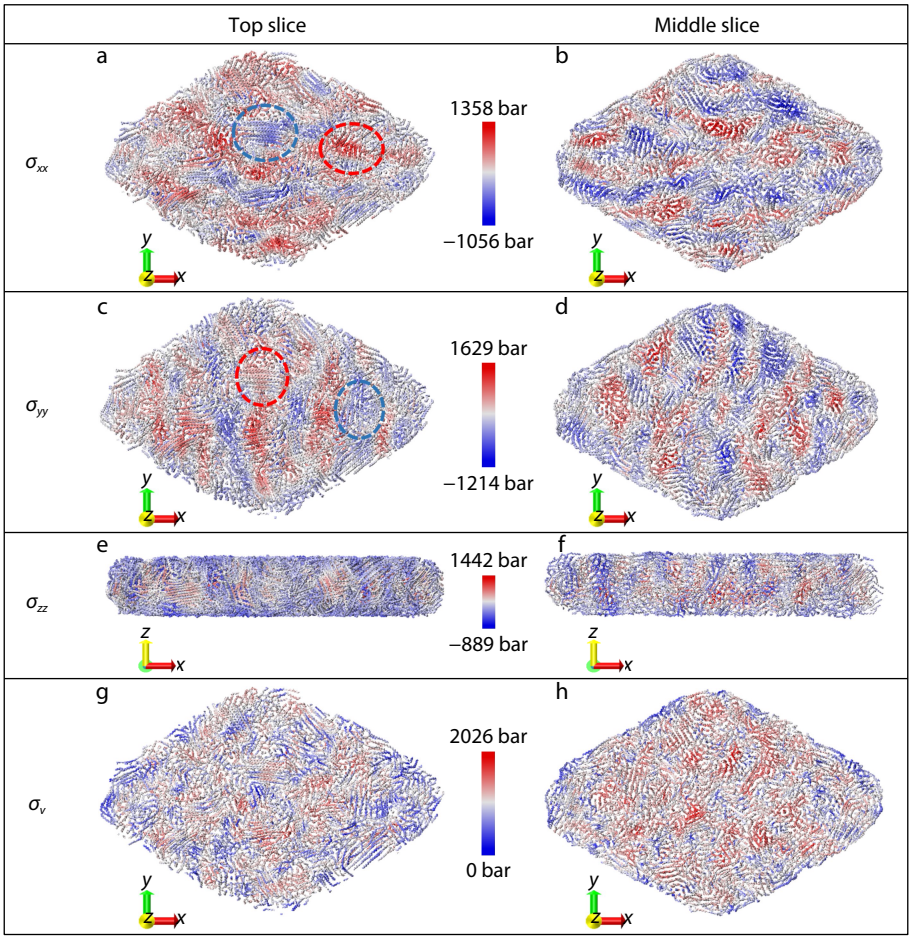


Fig. 7 Stress distribution of the semicrystalline polymer aggregates in template-4. We calculate the stress principals in *x* direction (σ_{xx}), *y* direction (σ_{yy}), *z* direction (σ_{zz}) and von Mises stress (σ_v). The top and middle slices of the spacial distribution are shown in the left and right columns, respectively.

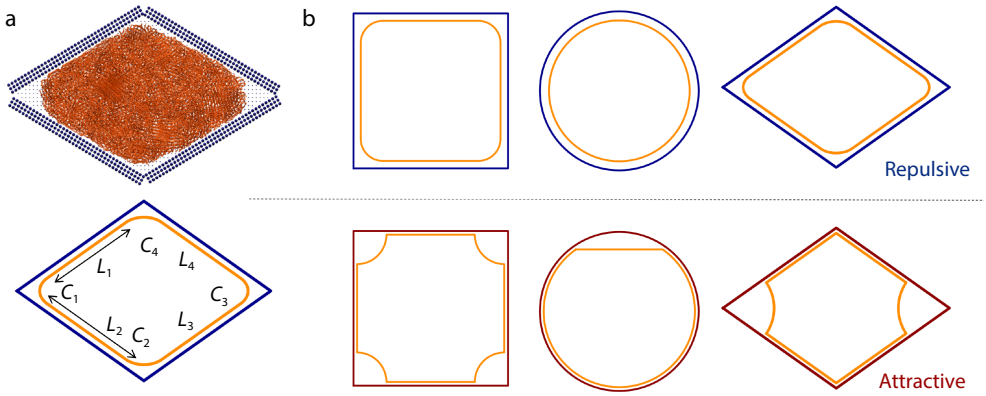


Fig. 8 (a) Illustration of a simplified 2D shape for polymer aggregates. The contour is modeled by four contact lines (L_1 to L_4) and four curves (C_1 to C_4). (b) Optimized shapes with minimum surface energy for repulsive and attractive templates, as shown in the upper and lower panels, respectively.

https://doi.org/10.1007/s10118-022-2712-6

both repulsive and attractive templates. Comparing with Fig. 2, we can see that the shapes obtained by simulations agree fairly well with the simple 2D model, with exceptions that regions near obtuse corners for attractive templates where the simulations may be trapped in a local minimum.

We do not find any obviously different conclusion from the structural parameters such as Q_6, P_z and N_e between the attractive and repulsive templates. The distribution of local stress is also found no apparent differences between the repulsive and attractive templates, except for the detailed values near corners.

CONCLUSIONS

We study the shape accuracy and residual stress distribution of nano-molded semicrystalline polymer, by using MD simulations. Four templates with different shapes are used to investigate the influences induced by template corners on the morphology of semicrystalline polymer flakes. Both repulsive and attractive templates are studied. We characterize the curvature of semicrystalline polymer flakes close to template corners and find the curvature decreases with corner angle. The curvature decreases during cooling process due to volume shrinkage, which indicates a decreasing effective interfacial affinity between polymers and templates at corners. A simple 2D shape model of minimum surface energy is proposed to describe the contour of semicrystalline polymers confined within templates. It is found that polymer chains at the upper and lower boundaries are more ordered than in the center. Highly ordered chain-packing is induced by the surface constraints where chains near the surfaces are orientated in *xy*-plane and perpendicular to *z*-axis. Moreover, we exhibit the spatial distribution of local stress for the semicrystalline polymer flakes to study the stress anisotropy according to the microstructure of polymer chains. The stress principal concentrates on chains oriented perpendicular to the present direction, for example, σ_{xx} concentrates on the areas where chains are oriented along y-axis, which is resulted from the squeezing induced by volume contraction during the cooling process primarily acting on the normal direction of the crystallized area. The von Mises stress is found primarily concentrated in the center of a polymer aggregate, which indicates surface compresses the center body due to volume shrinkage during the cooling process. There are two important factors which can affect the shape accuracy, crystalline structure and residual stress distribution: the confinement of nanoscale templates and the volume contraction during cooling. Our results provide a theoretical guidance to understand and improve the shape accuracy and mechanical properties of nanoscale polymer products.

NOTES

The authors declare no competing financial interest.

Electronic Supplementary Information

Electronic supplementary information (ESI) is available free of charge in the online version of this article at http://doi.org/10.1007/s10118-022-2712-6.

ACKNOWLEDGMENTS

This work was financially supported by the National Natural Science Foundation of China (Nos. 21873093, 21790340, 22073092 and 22103080), the National Key R&D Program of China (No. 2020YFA0713601), and the Key Research Program of Frontier Sciences, CAS (No. QYZDY-SSW-SLH027).

REFERENCES

1 Mohammadi, E.; Qu, G.; Kafle, P.; Jung, S. H.; Lee, J. K.; Diao, Y. Design rules for dynamic-template-directed crystallization of conjugated polymers. *Mol. Syst. Des. Eng.* **2020**, *5*, 125–138.
2 Michell, R. M.; Blaszczyk-Lezak, I.; Mijangos, C.; Müller, A. J. Confined crystallization of polymers within anodic aluminum oxide templates. *J. Polym. Sci., Part B: Polym. Phys.* **2014**, *52*, 1179–1194.
3 Shin, K.; Woo, E.; Jeong, Y. G.; Kim, C.; Huh, J.; Kim, K. W. Crystalline structures, melting, and crystallization of linear polyethylene in cylindrical nanopores. *Macromolecules* **2007**, *40*, 6617–6623.
4 Hu, Z.; Baralia, G.; Bayot, V.; Gohy, J. F.; Jonas, A. M. Nanoscale control of polymer crystallization by nanoimprint lithography. *Nano Lett.* **2005**, *5*, 1738–1743.
5 Cao, B. Y.; Yang, M.; Hu, G. J. Capillary filling dynamics of polymer melts in nanopores: experiments and rheological modelling. *RSC Adv.* **2016**, *6*, 7553–7559.
6 Michell, R. M.; Müller, A. J. Confined crystallization of polymeric materials. *Prog. Polym. Sci.* **2016**, *54–55*, 183–213.
7 Nakagawa, S.; Marubayashi, H.; Nojima, S. Crystallization of polymer chains confined in nanodomains. *Eur. Polym. J.* **2015**, *70*, 262–275.
8 Liu, G.; Müller, A. J.; Wang, D. Confined crystallization of polymers within nanopores. *Acc. Chem. Res.* **2021**, *54*, 3028–3038.
9 Maiz, J.; Martin, J.; Mijangos, C. Confinement effects on the crystallization of poly(ethylene oxide) nanotubes. *Langmuir* **2012**, *28*, 12296–12303.
10 Michell, R. M.; Blaszczyk-Lezak, I.; Mijangos, C.; Müller, A. J. Confinement effects on polymer crystallization: from droplets to alumina nanopores. *Polymer* **2013**, *54*, 4059–4077.
11 Lin, M. C.; Nandan, B.; Chen, H. L. Mediating polymer crystal orientation using nanotemplates from block copolymer microdomains and anodic aluminium oxide nanochannels. *Soft Matter* **2012**, *8*, 7306.
12 Huang, S.; Jiang, S. Structures and morphologies of biocompatible and biodegradable block copolymers. *RSC Adv.* **2014**, *4*, 24566–24583.
13 Jiang, Q.; Ward, M. D. Crystallization under nanoscale confinement. *Chem. Soc. Rev.* **2014**, *43*, 2066–2079.
14 Su, Y.; Liu, G.; Xie, B.; Fu, D.; Wang, D. Crystallization features of normal alkanes in confined geometry. *Acc. Chem. Res.* **2014**, *47*, 192–201.
15 Yung, K. L.; Kong, J.; Xu, Y. Studies on flow behaviors of polymer melts in nanochannels by wetting actions. *Polymer* **2007**, *48*, 7645–7652.
16 Woo, E.; Huh, J.; Jeong, Y. G.; Shin, K. From homogeneous to heterogeneous nucleation of chain molecules under nanoscopic cylindrical confinement. *Phys. Rev. Lett.* **2007**, *98*, 136103.
17 Duran, H.; Steinhart, M.; Butt, H. J.; Floudas, G. From heterogeneous to homogeneous nucleation of isotactic poly(propylene) confined to nanoporous alumina. *Nano Lett.*

2011, *11*, 1671–1675.
18 Suzuki, Y.; Duran, H.; Steinhart, M.; Butt, H. J.; Floudas, G. Homogeneous crystallization and local dynamics of poly(ethylene oxide) (PEO) confined to nanoporous alumina. *Soft Matter* **2013**, *9*, 2621–2628.
19 Wu, H.; Wang, W.; Huang, Y.; Su, Z. Orientation of syndiotactic polystyrene crystallized in cylindrical nanopores. *Macromol. Rapid Commun.* **2009**, *30*, 194–198.
20 Annicchiarico, D.; Alcock, J. R. Review of factors that affect shrinkage of molded part in injection molding. *Mater. Manuf. Process.* **2014**, *29*, 662–682.
21 Santis, F. D.; Pantani, R.; Speranza, V.; Titomanlio, G. Analysis of shrinkage development of a semicrystalline polymer during injection molding. *Ind. Eng. Chem. Res.* **2010**, *49*, 2469–2476.
22 Teng, C.; Li, L.; Wang, Y.; Wang, R.; Chen, W.; Wang, X.; Xue, G. How thermal stress alters the confinement of polymers vitrificated in nanopores. *J. Chem. Phys.* **2017**, *146*, 203319.
23 Guan, X.; Wang, J.; Hu, W. Monte carlo simulation of strain-enhanced stereocomplex polymer crystallization. *J. Phys. Chem. B* **2018**, *122*, 10928–10933.
24 Bresme, F.; Cámara, L. G. Computer simulation studies of crystallization under confinement conditions. *Chem. Geol.* **2006**, *230*, 197–206.
25 Cámara, L. G.; Bresme, F. Molecular dynamics simulations of crystallization under confinement at triple point conditions. *J. Chem. Phys.* **2003**, *119*, 2792–2800.
26 Cai, T.; Qian, Y.; Ma, Y.; Ren, Y.; Hu, W. Polymer crystallization confined in hard spherical microdomains of diblock copolymers. *Macromolecules* **2009**, *42*, 3381–3385.
27 Ming, Y.; Zhou, Z.; Zhang, S.; Wei, Y.; Hao, T.; Nie, Y. Molecular simulation of crystallization of polymers confined in cylindrical nanodomain. *Polymer* **2020**, *206*, 122818.
28 Hu, W.; Cai, T.; Ma, Y.; K. Hobbs, J.; Farrance, O.; Reiter, G. Polymer crystallization under nano-confinement of droplets studied by molecular simulations. *Faraday Discuss.* **2009**, *143*, 129–141.
29 Wang, M.; Hu, W.; Ma, Y.; Ma, Y. Q. Confined crystallization of cylindrical diblock copolymers studied by dynamic Monte Carlo simulations. *J. Chem. Phys.* **2006**, *124*, 244901.
30 Zhang, C.; Sha, Y.; Zhang, Y.; Cai, T.; Li, L.; Zhou, D.; Wang, X.; Xue, G. Nanostructures and dynamics of isochorically confined amorphous drug mediated by cooling rate, interfacial, and intermolecular interactions. *J. Phys. Chem. B* **2017**, *121*, 10704–10716.
31 Casas, M. T.; Michell, R. M.; Blaszczyk-Lezak, I.; Puiggali, J.; Mijangos, C.; Lorenzo, A. T.; Müller, A. J. Self-assembly of semicrystalline PE-*b*-PS diblock copolymers within AAO nanoporous templates. *Polymer* **2015**, *70*, 282–289.
32 Rigby, D.; Roe, R. J. Molecular dynamics simulation of polymer liquid and glass. I. Glass transition. *J. Chem. Phys.* **1987**, *87*, 7285.
33 Esselink, K.; Hilbers, P. A. J.; van Beest, B. W. H. Molecular dynamics study of nucleation and melting of *n*-alkanes. *J. Chem. Phys.* **1994**, *101*, 9033–9041.
34 Hess, B.; Kutzner, C.; van der Spoel, D.; Lindahl, E. GROMACS 4: algorithms for highly efficient, load-balanced, and scalable molecular simulation. *J. Chem. Theory Comput.* **2008**, *4*, 435–447.
35 Zhang, W.; Larson, R. G. Effect of flow-induced nematic order on polyethylene crystal nucleation. *Macromolecules* **2020**, *53*, 7650–7657.
36 Gao, H.; Menzel, T. P. W.; Müser, M. H.; Mukherji, D. Comparing simulated specific heat of liquid polymers and oligomers to experiments. *Phys. Rev. Mater.* **2021**, *5*, 065605.
37 Kass, M.; Witkin, A.; Terzopoulos, D. Snakes: active contour models. *Int. J. Comput. Vis.* **1988**, *1*, 321–331.
38 Steinhardt, P. J.; Nelson, D. R.; Ronchetti, M. Bond-orientational order in liquids and glasses. *Phys. Rev. B* **1983**, *28*, 784–805.
39 Lechner, W.; Dellago, C. Accurate determination of crystal structures based on averaged local bond order parameters. *J. Chem. Phys.* **2008**, *129*, 114707.
40 Luo, C.; Kröger, M.; Sommer, J. U. Entanglements and crystallization of concentrated polymer solutions: molecular dynamics simulations. *Macromolecules* **2016**, *49*, 9017–9025.
41 Everaers, R.; Sukumaran, S. K.; Grest, G. S.; Svaneborg, C.; Sivasubramanian, A.; Kremer, K. Rheology and microscopic topology of entangled polymeric liquids. *Science* **2004**, *303*, 823–826.
42 Luo, C.; Kröger, M.; Sommer, J. U. Molecular dynamics simulations of polymer crystallization under confinement: entanglement effect. *Polymer* **2017**, *109*, 71–84.
43 Vanegas, J. M.; Torres-Sánchez, A.; Arroyo, M. Importance of force decomposition for local stress calculations in biomembrane molecular simulations. *J. Chem. Theory Comput.* **2014**, *10*, 691–702.
44 Ollila, O. H. S.; Risselada, H. J.; Louhivuori, M.; Lindahl, E.; Vattulainen, I.; Marrink, S. J. 3D pressure field in lipid membranes and membrane-protein complexes. *Phys. Rev. Lett.* **2009**, *102*, 078101.

https://doi.org/10.1007/s10118-022-2712-6